Scripta Materialia 246 (2024) 116067

Contents lists available at ScienceDirect

Scripta Materialia

journal homepage: www.journals.elsevier.com/scripta-materialia

Wetting of $L1_0$ twin and antiphase boundaries by nanometer-scale $L1_2$ in Fe-Pd alloys

Adrian Savovici [a,*], Yongmei M. Jin [b], William A. Soffa [a], Jerrold A. Floro [a]

[a] Department of Materials Science and Engineering, University of Virginia, 395 McCormick Road, Charlottesville, VA 22904, USA
[b] Department of Materials Science and Engineering, Michigan Technological University, 1400 Townsend Drive, Houghton, MI 49931, USA

ARTICLE INFO

Keywords:
Magnetic Fe-Pd alloy
Polytwin structure
Orientation domain boundary
Antiphase boundary
Nanometer-scale interface

ABSTRACT

This paper reports microstructure associated with the $L1_0$ and $L1_2$ two-phase coexistence region in magnetic Fe-Pd alloys and analyzes the observed complex nanometer scale wetting layer structures. Fe - 61.8 at% Pd samples were continuously cooled from the disordered A1 phase through the eutectoid isotherm and aged at 650 °C for various times. X-ray diffraction reveals that the samples first order to $L1_2$ then transform to $L1_0$-dominant $L1_0 + L1_2$ two-phase mixture. It is shown that $L1_0$ forms {110} polytwin microstructure with straight $\{1\bar{1}0\}$ antiphase boundaries (APBs), where $L1_2$ exists as nanometer-scale wetting layers along the twin boundaries and APBs. The variant selection for $L1_2/L1_0$ wetting layers is discussed, and evidence of closed/open APB structures is shown with high-resolution transmission electron microscopy.

The $L1_0$ ordered phase has long been studied as a potential permanent magnet in Co-Pt, Fe-Pt, Fe-Pd, and Mn-Al binary alloys due to its high uniaxial magnetocrystalline anisotropy [1]. Tetragonal $L1_0$ (P4/mmm, Pearson symbol tP2, see Fig. 1a) is usually studied at or near the equiatomic composition. The $L1_0$ (AB) phase field may be bracketed by cubic $L1_2$ phase fields (A_3B & AB_3, $Pm\bar{3}m$, Pearson symbol cP4, see Fig. 1a). The $L1_0$-$L1_2$ coexistence regions may only span 2–5 at% in width and are connected by a eutectoid reaction $A1 \rightarrow L1_0 + L1_2$. Despite their potential as self-assembled exchange coupled ferromagnets, many of these two-phase coexistence regions are still poorly characterized – the solvus boundaries are often estimated, and the two-phase microstructures are unexplored but potentially of significant interest. For example, in Co-Pt, strain-induced ordering produces a unique nanochessboard [2] morphology that can foster effective exchange coupling between the anisotropic $L1_0$ phase with $L1_2$ [3–5]. Another interesting two-phase microstructure is observed in Co-Pt where $L1_0$ twin interfaces are wetted by nanometer-scale $L1_2$ layers and antiphase boundaries (APBs) exhibit a $L1_2/L1_0/L1_2$ trilayer structure [6]. The equivalent two-phase region in Fe-Pd has not been explored, and is of interest since the smaller c/a ratio associated with the unit cell (relative to Co-Pt) is predicted to modify the resultant microstructure [7]. Furthermore, Fe-Pd has a lower magnetocrystalline anisotropy than Co-Pt, which impacts the length scales over which exchange-coupled ferromagnetism can occur. Recently, it was also shown that Fe-Pd can order to the L1' structure first predicted by Shockley, see Fig. 1a [8–10].

Bulk Fe-Pd $L1_0$ alloys self-assemble into the so-called polytwin microstructure, which forms as a means of reducing the transformation strain energy accrued during the cubic→tetragonal transformation from A1 [11,12]. As shown in Fig. 1b, a prototypical $L1_0$ polytwin colony consists of alternating conjugate pairs of $L1_0$ orientation variants whose c-axes (shown as the double headed arrows) lie along two of the three ⟨100⟩ directions of the parent A1 phase. Note that the layer structure shown in Fig. 1b was referred to as a "plate" by Vlasova, et al. [13], but since this terminology has potential for confusion, we will adopt "colony" as a descriptor instead. The term "plate" will be used to refer to a bounded region containing one or multiple "colonies" (see Fig. 3a). The twin boundaries separating the $L1_0$ orientation variants are coherent {110} planes which we will refer to as orientation domain boundaries (ODBs). These boundaries have also been referred to as orientation domain walls, but we adopt the ODB notation since it better highlights the differences (and similarities) with boundaries that separate antiphase domains (i.e., translational variants), within a single orientation variant, i.e., APBs.

Fig. 1c shows a schematic of the $L1_0 + L1_2$ microstructure observed in our current Fe - 61.8 at% Pd samples in the two-phase coexistence region. It exhibits similar polytwin structure in the $L1_0$ matrix, but ODBs and APBs are wetted with thin layers of $L1_2$ (blue colored solid and dashed lines). Note that the APBs herein are facetted along $\{1\bar{1}0\}$

* Corresponding author.
E-mail address: as5fj@virginia.edu (A. Savovici).

https://doi.org/10.1016/j.scriptamat.2024.116067
Received 30 November 2023; Received in revised form 29 January 2024; Accepted 5 March 2024
Available online 16 March 2024

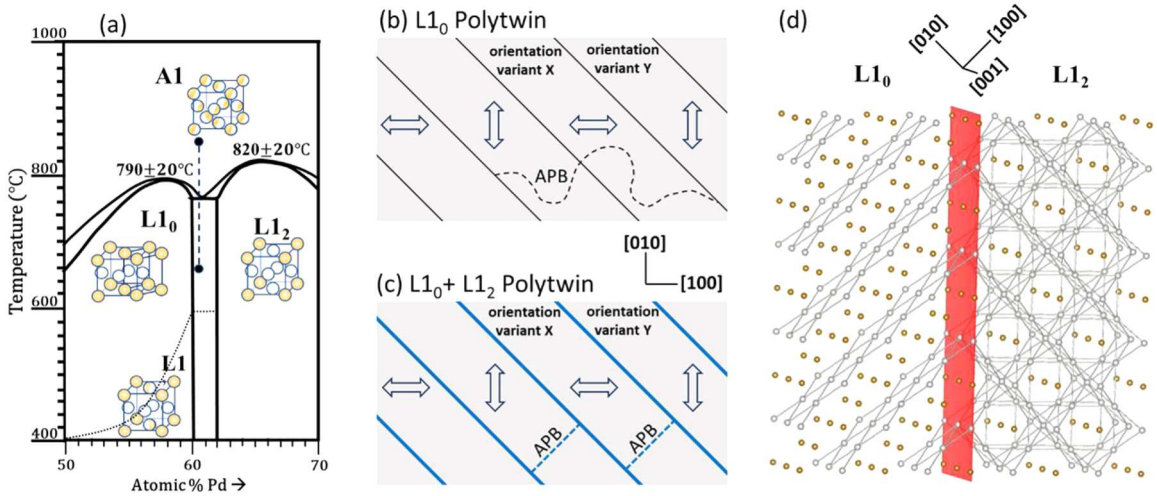

Fig. 1. (a) A snippet of the Fe-Pd phase diagram near the two-phase coexistence region, adapted from [ref. 8]. Also included is the transition from $L1_0 \rightarrow L1'$ at lower temperatures (the transformation boundary shown in dashes is largely schematic). (b,c) Schematic (110) polytwin structures of single phase $L1_0$ in (b) and $L1_0$+$L1_2$ two-phase microstructure with $L1_2$ wetting layers in (c). The blue solid lines along ODBs and blue dashed lines along APBs represent the $L1_2$ wetting layers. (d) A schematic of atomic coherency at an $L1_0/L1_2$ (110) interface showing continuity of Pd (002) sheets from $L1_0$ into $L1_2$ (the model is tilted for better view of the interface). The gold and white atoms are Fe and Pd, respectively.

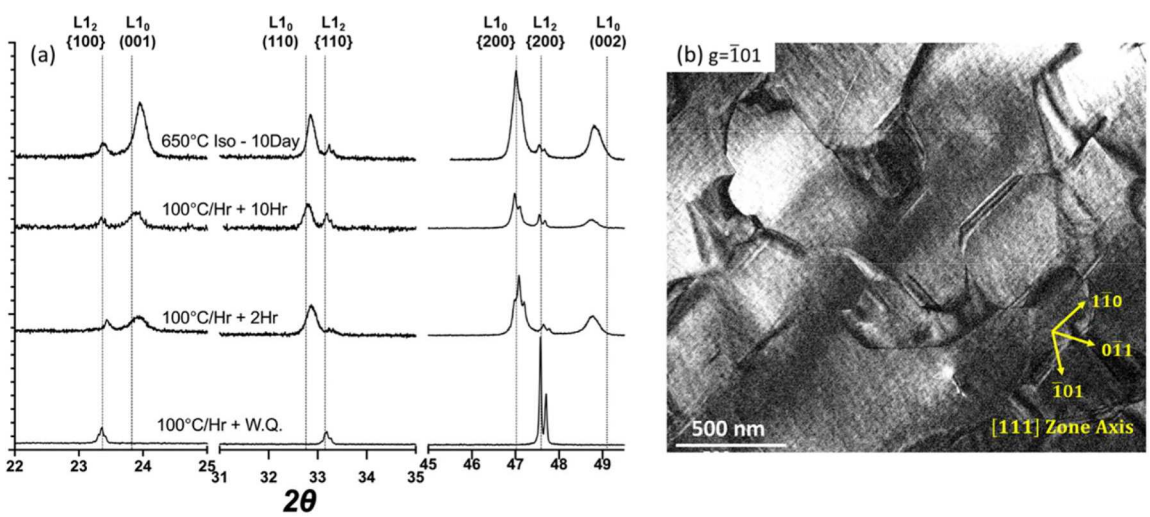

Fig. 2. (a) X-ray diffraction patterns of Fe – 61.8 at% Pd samples for different processing conditions. The scale of the superlattice reflection intensities are about 3X larger than the {200} fundamental, for clarity. (b) DF-TEM micrograph of a sample processed as 100 °C/hr + 30 min sample, which exhibits single-phase $L1_2$.

perpendicular to the ODBs, unlike the 'transformation APBs' that usually appear to be curvilinear [1,12] as schematically illustrated in Fig. 1b. These $\{1\bar{1}0\}$ APBs will be shown to have a complex multilayer structure because of the variant selection rule for $L1_0$-$L1_2$ wetting layers [6,14]. Fig. 1d exemplifies low-energy alignment of $L1_0$ and $L1_2$ phases where Pd-rich (002) sheets are continuous across the {110} interface, which will be discussed later in connection with the variant selection rule and the structure of wetting layers.

An Fe-Pd boule was arc-melted from 99.99 % Fe and 99.9 % Pd chunks in an argon-backfilled ambient environment, with a nominal composition of 61.8 at% Pd. The resulting composition was verified by inductively-coupled optical emission spectroscopy. Repeated cold-rolling and recrystallization with 24hr homogenization at 1000 °C yielded samples of ~300μm thickness. Samples were encapsulated in quartz ampoules, backfilled with forming gas, annealed in tube furnaces, then water quenched. Structural analysis was performed using X-ray diffraction (XRD) and transmission electron microscopy (TEM). Details are provided elsewhere [9].

Samples were continuously cooled from 850 °C to 650 °C through the eutectoid isotherm (~760 °C) at rates of 50–400 °C/hr to drive the phase transformation. Water quenching after the cooling process invariably produced only single-phase $L1_2$ with no residual A1 detected in the lowermost diffraction pattern in Fig. 2a. However, for samples aged after the initial continuous cool treatment, $L1_0$ grew at the expense of the $L1_2$ matrix (one such $L1_2$ matrix region is given in Fig. 2b). TEM imaging in Fig. 2b, and Figs. S1 and S2 of Supporting Information, confirms the presence of $L1_2$, with characteristic APBs across extended areas. While no evidence of $L1_0$ is apparent via XRD, dark-field TEM (DF-TEM) does show so-called tweed contrast in the $L1_2$ (Fig. 2b). This type of contrast is observed in many cubic→tetragonal transformations where a high density of correlated tetragonal strain centers emerge in the cubic parent phase. This coherent assembly produces a net matrix strain often dominated by $\{110\} < 1\bar{1}0 >$ displacement waves in the elastically anisotropic matrix, giving rise to strain-contrast striations along the traces of the {110} planes of the parent matrix in TEM. These premonitory fluctuations indicate an incipient phase change, that will ultimately lead here to formation of $L1_0$ from the supersaturated $L1_2$.

Additional isothermal annealing at 650 °C subsequently produces

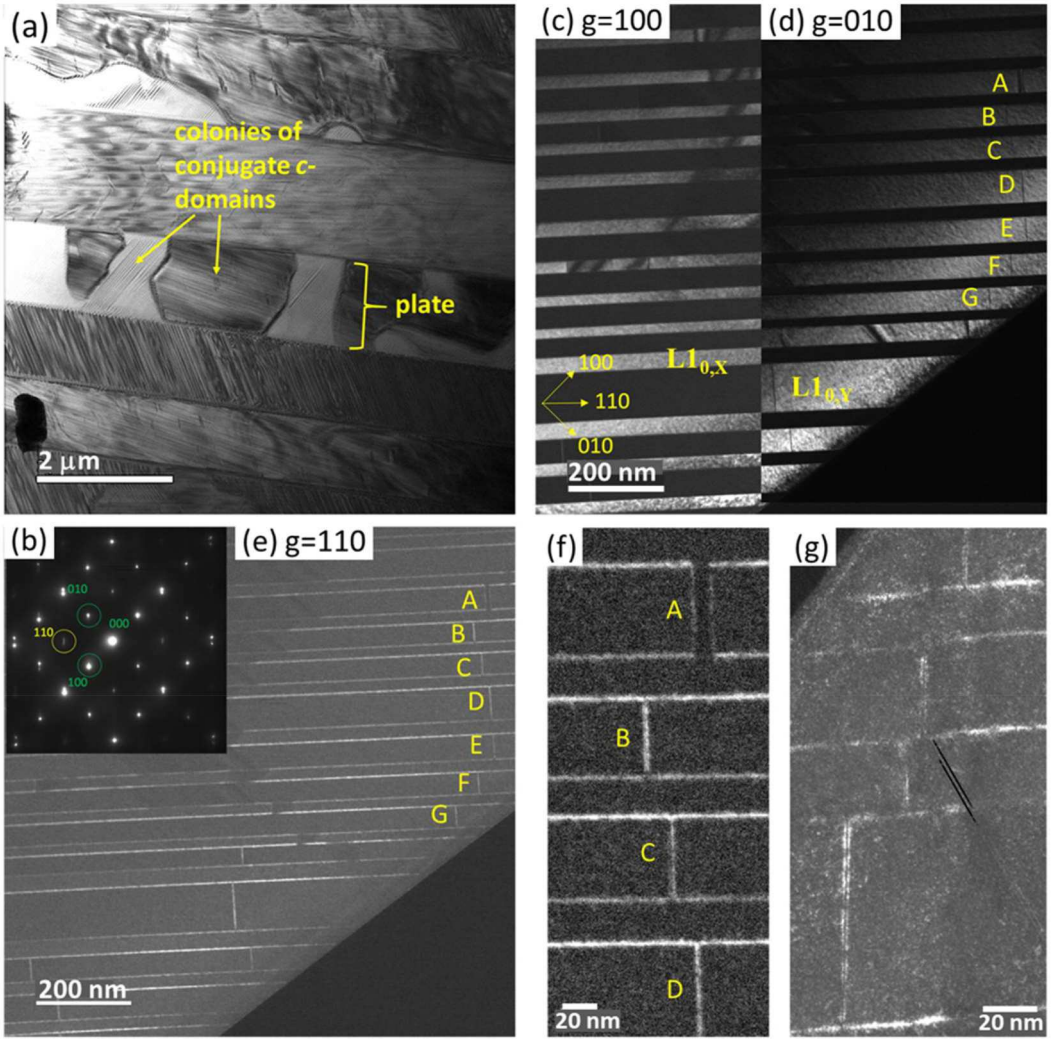

Fig. 3. Fe - 61.8 at% Pd alloys after 100 °C/hr + 2hr processing. (a) Overall microstructure consists of multiple polytwin colonies. In (b-e), the same region is imaged. An SADP on a [001] zone axis is shown in (b), with identification of the (010), (100), and (110) superlattice reflections. DF imaging in (c) with $g = 100$ and (d) $g = 010$ assigns $L1_0$ orientation variants as $L1_{0,X}$ & $L1_{0,Y}$, respectively. Imaging with $g = 110$ in (e) highlights the $L1_2$ phase, which exists solely as a wetting layer along $L1_0$ ODBs and APBs. DF images at higher magnification in (f) and (g) reveal the central channel of the complex APB structure.

order-order decomposition, $L1_2 \rightarrow L1_0 + L1_2$. Fig. 2 summarizes XRD evidence for two-phase coexistence in samples cooled from 850→650 °C at 100 °C/hr, then aged for 2 and 10 hrs. at 650 °C. Fundamental and superlattice peaks from $L1_0$ and $L1_2$ are distinctly identified. The lattice constants extracted from a satisfactory Rietveld Refinement fit (in GSAS-II [15]) of the isothermally aged sample are $a_{L10} = 3.873A$ and $c_{L10} = 3.739A$ while $a_{L12} = 3.832A$. The dashed lines in Fig. 2 are placed at 2θ locations generated from single-phase samples. They are not identical with the lattice constants in these two-phase samples due to coherency strains, as found in Co-Pt [4], and perhaps small differences in alloy composition. Nonetheless, we are confident in these peak assignments. Fig. 2 additionally shows that a sample that was directly isothermally aged for 10 days at 650 °C after quenching in the A1 solid solution phase, also displayed $L1_0 + L1_2$ coexistence.

Fig. 3 shows the characteristic microstructure for the two-phase coexistence. Each grain consisted of polytwinned $L1_0$ plates (Fig. 3a). A selected area diffraction pattern (SADP) with [001] zone axis is shown in Fig. 3b and dark-field micrographs using different ***g***-vectors for imaging are shown in Fig. 3c,d,e. In this region, the {110} ODBs and $\{1\bar{1}0\}$ APBs are oriented edge-on to the [001] zone axis. In DF mode, assignment of the $L1_0$ orientation variants can be readily made since the *c*-axes of the conjugate pair of orientation variants are nearly orthogonal to one, as shown in Fig. 1b,c. For convenience, the orientation variants will be named as $L1_{0,X}$, $L1_{0,Y}$, and $L1_{0,Z}$, according to the c-axis orientation in [100], [010], and [001] directions of the A1 parent, respectively. As such, the (100) and (010) reflections in the SADP of Fig. 3b arise from the $L1_{0,X}$ and $L1_{0,Y}$ variants, respectively, producing bright regions in DF images using $\boldsymbol{g} = 100$ in Fig. 3c ($L1_{0,X}$) and $\boldsymbol{g} = 010$ in Fig. 3d ($L1_{0,Y}$). Fig. 3e is particularly important. DF imaging using $\boldsymbol{g} = 110$ will not illuminate either of the present $L1_0$ orientation variants, but $L1_2$ will be illuminated. Fig. 3e shows that $L1_2$ exists as thin, continuous layers wetting ODBs and APBs (as illustrated in Fig 1c). In Fig. 3b the (110) reflection is weak compared to the (100) and (010) reflections and appears as a rel-rod, consistent with $L1_2$ as a minority phase present only in the form of very thin wetting layers.

Consider the APBs labeled as A-G in Fig. 3e, where $\boldsymbol{g} = 110$ identifies the presence of an $L1_2$ wetting layer at each of them. Comparing with Fig. 3d using $\boldsymbol{g} = 010$, a narrow dark band exists at the corresponding APB locations. Since, the bright domains are $L1_{0,Y}$ variant, A-G are the $L1_{0,Y}$-type APBs between $L1_{0,Ya}$ and $L1_{0,Yb}$ variants. The dark contrast of these narrow bands indicates the presence of an $L1_{0,X}$ channel at the center of the $L1_{0,Y}$ type APBs that are $L1_2$-wetted, and will be discussed below. It is also found that the narrow $L1_{0,X}$ channel at each APB provides a connection between the two neighboring $L1_{0,X}$ variants at either *end* of the APBs, one above and one below. APB "A" (located near the

Table 1
$L1_0/L1_2$ Variant Selection.

$L1_0$ Variant	$L1_2$ Variant
$L1_{0,Xa}$	$L1_{2,a}$ or $L1_{2,b}$
$L1_{0,Xb}$	$L1_{2,c}$ or $L1_{2,d}$
$L1_{0,Ya}$	$L1_{2,a}$ or $L1_{2,c}$
$L1_{0,Yb}$	$L1_{2,b}$ or $L1_{2,d}$
$L1_{0,Za}$	$L1_{2,a}$ or $L1_{2,d}$
$L1_{0,Zb}$	$L1_{2,b}$ or $L1_{2,c}$

upper right corner of Figs. 3d,e) has an $L1_0$ channel that is quite thick and is readily resolved. This APB is shown in higher detail in Fig. 3f in a higher magnification DF image using $\boldsymbol{g} = 110$. Fig. 3g shows a DF image from a different region where narrow channels are resolved. We next discuss the APB structure in more detail.

To analyze the interfaces between the multiple variants of ordered $L1_0$ and $L1_2$ phases, we must name the variants unambiguously. The reduced translational symmetry of $L1_0$ vs. the parent FCC means that for every orientation variant, $L1_{0,X}$, $L1_{0,Y}$, $L1_{0,Z}$, there are only 2 translational (or antiphase) variants in $L1_0$, producing 6 possible $L1_0$ variants. We name them $L1_{0,Xa}$, $L1_{0,Xb}$, $L1_{0,Ya}$, $L1_{0,Yb}$, $L1_{0,Za}$, $L1_{0,Zb}$, where 'a' designates the translation variants with Fe sheet at (0,0,0) and 'b' with Pd sheet at (0,0,0); see Fig. S3 for more details. Cubic $L1_2$ does not form orientation variants, but as it can order on the parent FCC lattice on any of four sublattice sites, we name the four translation variants as $L1_{2,a}$, $L1_{2,b}$, $L1_{2,c}$, $L1_{2,d}$, based on the Fe atom positioning at (0,0,0), (0,1/2,1/2), (1/2,0,1/2), (1/2,1/2,0), respectively. Wetting in Co-Pt alloys was shown to form energetically favorable $L1_0/L1_2$ interfaces by following a simple geometrical rule that ensures continuation of (002) Pd-rich planes across $L1_0/L1_2$ interfaces [6,14]. This allows only certain $L1_2$ translation variants for each $L1_0$ variant, as listed in Table I. Applying the variant selection rule for the layers wetting the $L1_0$ ODB's is simple: in Table 1, for any possible $L1_0$ orientation variant pair (total 12), there is always one common $L1_2$ variant that is favored by both. For example, $L1_{2,a}$ is favored by both $L1_{0,Xa}$ and $L1_{0,Ya}$, thus the wetting behavior at the $L1_{0,Xa}$-$L1_{0,Ya}$ OBD simply leads to a wetting layer with $L1_{2,a}$ structure. The complex APB channel structure observed in Fig. 3 can also be explained by application of the $L1_0/L1_2$ variant selection rule.

It is seen from Table 1 that, for any pair of antiphase domains (a total of 3 possible pairs, one for each orientation variant), there is no common $L1_2$ variant favored by both. Consider the $L1_{0,Ya}$-$L1_{0,Yb}$ type APB as an example. $L1_{0,Ya}$ favors $L1_{2,a}$ or $L1_{2,c}$ while $L1_{0,Yb}$ favors $L1_{2,b}$ or $L1_{2,d}$. The wetting layer for an $L1_{0,Ya}$ - $L1_{0,Yb}$ APB necessitates different $L1_2$ variants, and there are two interface options for this scenario: either an $L1_2$ APB is formed between different $L1_2$ wetting layers, or an $L1_0$ variant layer favored by both $L1_2$ variants forms in the middle. The latter corresponds to a three-layer APB structure of $L1_2/L1_0/L1_2$, which is energetically more favorable [6,14].

An $L1_0$ APB with $L1_2$ wetting therefore has, at its center, a layer of its conjugate $L1_0$ orientation variant. This explains the observation of $L1_{0\text{-}X}$ narrow channels at the APBs in the $L1_{0\text{-}Y}$ regions in Fig. 3d. Since, the central $L1_{0,X}$ layer is sandwiched between two adjoining $L1_{0,Y}$ antiphase domains, stress accommodation dictates the layer to be planar and orient along {110} planes which are the misfit-free planes between two tetragonal orientation domains. This is consistent with the observations of straight APBs (compare curvilinear and straight APBs in Fig. 1b,c) and their orientations along $\{1\bar{1}0\}$ perpendicular to the ODBs. Such a complex APB presents as a channel, since it is connected to adjacent $L1_{0,X}$ domains at either end. While the $L1_0$ channel and the two connected $L1_0$ orientation domains at either end are of the same orientation type, they can be translationally in- or out-of-phase with respect to one another, which should influence channel structure.

Consider a vertically-oriented APB and its lower end part as schematically illustrated in Fig. 4a,b. Grey regions correspond to one $L1_0$

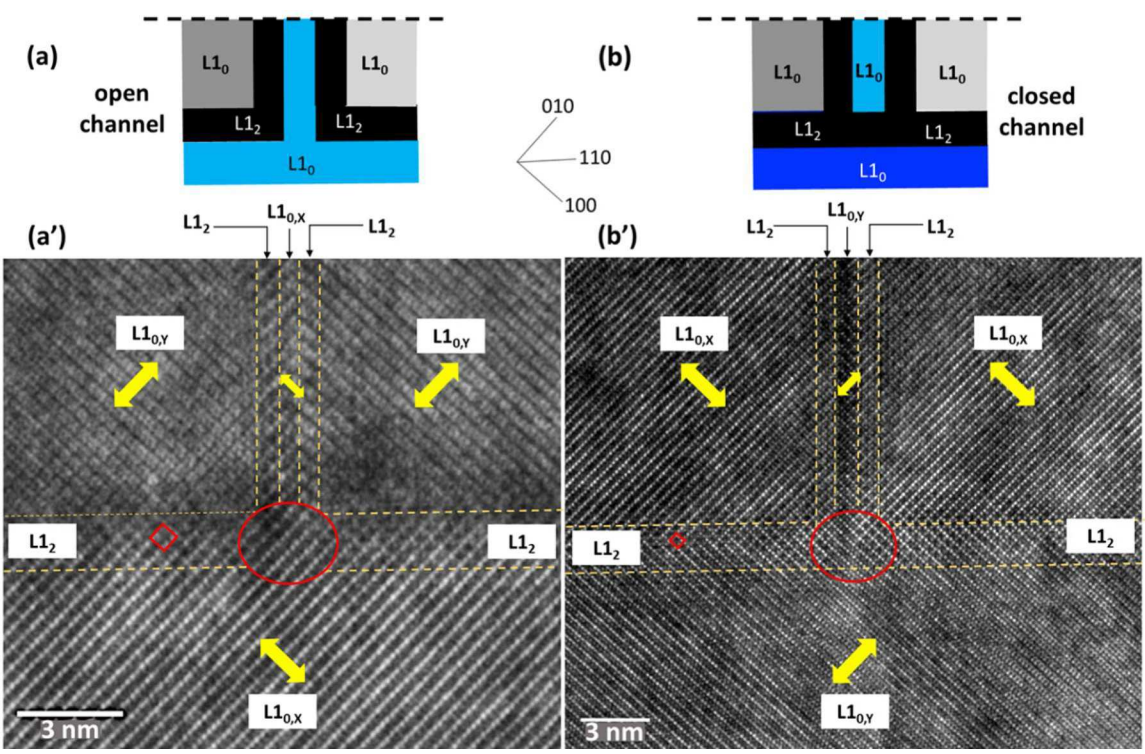

Fig. 4. Schematics (a,b) and HRTEM micrographs (a',b') of complex APB and ODB wetting structure. (a,a') Open channel structure, where the central channel $L1_0$ variant is orientationally and translationally continuous with the $L1_0$ variant below. (b,b') Closed channel structure, where the central channel $L1_0$ variant is orientationally continuous but translationally discontinuous with the $L1_0$ variant below. The dotted lines bound the cubic wetting layer on ODBs & APBs. Large arrows depict the *c*-axis orientation in each variant, while that of the central $L1_0$ channel region is identified by a small arrow. Red ovals highlight where open or closed APB structure forms.

orientation variant, blue regions designate the conjugate $L1_0$ orientation domain, and the black regions correspond to the $L1_2$ wetting layer along the ODB and APBs. When the central channel $L1_0$ variant is translationally in-phase with the $L1_0$ variant below, they connect directly and the channel is said to be an "open" structure in Fig. 4a. In contrast, when the central channel $L1_0$ variant is translationally out-of-phase with the $L1_0$ variant below, they cannot connect directly and rather than forming an APB, a continuation of the wetting $L1_2$ layer is present instead. The channel is thus blocked by a layer of $L1_2$ and forms a "closed" structure, as seen in Fig. 4b. These structures, predicted using the variant selection rule, are indeed observed using High Resolution TEM (HRTEM) (see the micrographs in Fig. 4a,b). The $L1_0$ and $L1_2$ phase regions as well as the *c*-axis orientations (by the double headed arrows) of the $L1_0$ orientation variants are identified, and their boundaries are highlighted with dashed lines, which helps visualize the ODBs and APBs. Examining the end parts of the APBs highlighted by red ovals, the $L1_0$ fringe pattern below is seen to be extended up to the APB wetting layer in Fig. 4a' while the $L1_2$ fringe pattern is seen to separate the APB above and the $L1_0$ variant below in Fig. 4b'. Clearly, the former agrees with the open channel structure in Fig. 4a while the latter agrees with the closed channel structure in Fig. 4b. The effects of such unusual APB and ODB wetting structures with open channels and closed channels on magnetic properties deserve future investigation.

In summary, we report the first structural and microstructural probe of $L1_0 + L1_2$ two-phase alloys in Fe – 61.8 at% Pd samples. Continuous cooling through the eutectoid isotherm from solid solution progressed via an interesting pathway, where all samples first ordered to single-phase $L1_2$ then decomposed into a majority $L1_0$ phase, with minority $L1_2$ found to exist only as a wetting layer along $L1_0$ ODBs and {110}-aligned APBs within the polytwinned microstructure. Similar microstructure was observed previously in $Co_{40}Pt_{60}$, but the transformation path progressed by first ordering to $L1_0$ [6]. This suggests there are two distinct structural evolution pathways which give rise to microstructures observed in Fe-Pd and Co-Pt systems. Interestingly, an $L1_2$-first pathway to $L1_0 + L1_2$ coexistence in $Co_{38.5}Pt_{61.6}$ alloys produced a majority $L1_2$-phase microstructure where $L1_2$ APBs were decorated with wetting $L1_0$ layers (single-layer and curvilinear) [14]. In the current work, use of the variant selection rule for $L1_0/L1_2$ interfaces explains the observations of the {110} faceted $L1_0$ APBs with $L1_2/L1_0/L1_2$ three-layer structure. The structural analysis further predicts a peculiar feature of these three-layer $L1_0$ APBs, namely open and closed $L1_0$ channel structures, which present a previously undiscussed level of complexity. Both open and closed $L1_0$ channel structures are identified using HRTEM images.

Extensive use of the UVA Nanoscale Materials Characterization Facility is greatly appreciated. This work was supported by the National Science Foundation under Grant DMR-1709914 (A.S., W.A.S, and J.A.F) and CMMI-2212324 (Y.M.J.).

Declaration of competing interest

The authors declare that they have no known competing financial interests or personal relationships that could have appeared to influence the work reported in this paper.

Supplementary materials

Supplementary material associated with this article can be found, in the online version, at doi:10.1016/j.scriptamat.2024.116067.

References

[1] T. Klemmer, D. Hoydick, H. Okumura, B. Zhang, W.A. Soffa, Magnetic hardening and coercivity mechanisms in L10 ordered FePd ferromagnets, Scripta Met. Mater. 33 (10) (1995) 1793–1805, https://doi.org/10.1016/0956-716X(95)00413-P.
[2] C. Leroux, A. Loiseau, D. Broddin, G. Vantendeloo, Electron microscopy study of the coherent two-phase mixtures L10+ L12, in Co–Pt alloys, Philos. Mag. B 64 (1) (1991) 57–82, https://doi.org/10.1080/13642819108207603.
[3] E. Vetter, P. Ghatwai, W. Soffa, J. Floro, Evolution of first-order reversal curves during self-assembly of the $Co_{40.2}Pt_{59.8}$ nano-chessboard structure, IEEE Magn. Lett. 6 (2015) 1–4, https://doi.org/10.1109/LMAG.2015.2480386.
[4] J.A. Floro, E.P. Vetter, P. Ghatwai, L.D. Geng, Y.M. Jin, W.A. Soffa, Hierarchical structure and the origins of coercivity in exchange-coupled Co-Pt nanochessboards, J. Magn. Magn. Mater. 487 (2019) 165313, https://doi.org/10.1016/j.jmmm.2019.165313.
[5] L.D. Geng, W.A. Soffa, J.A. Floro, Y.M. Jin, Exchange coupling effects in Co-Pt nanochessboards, J. Appl. Phys. 123 (9) (2018) 093901, https://doi.org/10.1063/1.5019841.
[6] Y. Le Bouar, A. Loiseau, A Finel, Origin of the complex wetting behavior in Co-Pt alloys, Phys. Rev. B 68 (22) (2003) 224203, https://doi.org/10.1103/PhysRevB.68.224203.
[7] Y. Ni, A.G. Khachaturyan, From chessboard tweed to chessboard nanowire structure during pseudospinodal decomposition, Nat. Mater. 8 (5) (2009) 410–414, https://doi.org/10.1038/nmat2431.
[8] M.A. Steiner, R.B. Comes, J.A. Floro, W.A. Soffa, J.M. Fitz-Gerald, L1′ ordering: evidence of L10–L12 hybridization in strained Fe38.5Pd61.5 epitaxial films, Acta Mater 85 (2015) 261–269, https://doi.org/10.1016/j.actamat.2014.11.036.
[9] A. Savovici, W.A. Soffa, J.A. Floro, Direct evidence of the shockley tetragonal L1' phase in a bulk Fe-Pd alloy, Scr. Mater. 234 (2023) 115540, https://doi.org/10.1016/j.scriptamat.2023.115540.
[10] W. Shockley, Theory of order for the copper gold alloy system, J. Chem. Phys. 6 (3) (2004) 130–144, https://doi.org/10.1063/1.1750214.
[11] M. Hirabayashi, S. Weissmann, Study of CuAu I by transmission electron microscopy, Acta Metall 10 (1) (1962) 25–36, https://doi.org/10.1016/0001-6160(62)90183-9.
[12] B. Zhang, W.A. Soffa, Magnetic domains and coercivity in polytwinned ferromagnets, Phys. Status Solidi A 131 (2) (1992) 707–725, https://doi.org/10.1002/pssa.2211310239.
[13] N.I. Vlasova, G.S. Kandaurova, N.N. Shchegoleva, Effect of the polytwinned microstructure parameters on magnetic domain structure and hysteresis properties of the CoPt-type alloys, J. Magn. Magn. Mater. 222 (1) (2000) 138–158, https://doi.org/10.1016/S0304-8853(00)00506-0.
[14] Y. Le Bouar, A. Loiseau, A. Finel, F Ducastelle, Wetting behavior in the Co-Pt system, Phys. Rev. B 61 (5) (2000) 3317–3326, https://doi.org/10.1103/PhysRevB.61.3317.
[15] B.H. Toby, R.B.GSAS-II Von Dreele, The genesis of a modern open-source all purpose crystallography software package, J. Appl. Crystallogr. 46 (2) (2013) 544–549, https://doi.org/10.1107/S0021889813003531.